

# Magnetoresistance and Hall effect near the metal-insulator transition of $\text{Cd}_{1-x}\text{Mn}_x\text{Se}$

Y. Shapira

*Francis Bitter National Magnet Laboratory and the Department of Physics, Massachusetts Institute of Technology, Cambridge, Massachusetts 02139*

N. F. Oliveira, Jr.

*Instituto de Física, Universidade de São Paulo, Caixa Postal 20 516, 05 508 São Paulo, São Paulo, Brazil and Francis Bitter National Magnet Laboratory, Massachusetts Institute of Technology, Cambridge, Massachusetts 02139*

D. H. Ridgley, R. Kershaw, K. Dwight, and A. Wold

*Department of Chemistry, Brown University, Providence, Rhode Island 02912*

(Received 10 February 1986)

Resistivity and Hall measurements were made on  $n$ -type  $\text{Cd}_{1-x}\text{Mn}_x\text{Se}$  samples with  $x=0.01$ ,  $0.05$ , and  $0.10$  at temperatures  $0.3 \leq T \leq 300$  K and in magnetic fields  $H \leq 80$  kOe. For each value of  $x$ , several samples with different room-temperature carrier concentrations  $n_{\text{RT}}$  were studied. They cover the range from slightly below  $n_c$  to  $n > n_c$ , where  $n_c$  is the carrier concentration at the metal-insulator transition. The zero-field data indicate that for samples grown in the same manner  $n_c$  increases with increasing  $x$ . For  $T \leq 4.2$  K a large magnetoresistance (MR), and large changes in the Hall coefficient  $R$  with  $H$ , are observed. In some cases the  $H$ -induced change in the resistivity exceeds a factor of 10. At low  $H$  the MR is always positive. For samples with  $x=0.05$  and  $0.10$  the MR goes through a maximum at a field  $H_{\text{max}}$ , and it then decreases at higher  $H$ . The value of  $H_{\text{max}}$  decreases with decreasing  $T$ . For  $x=0.01$  the resistivity at  $T \geq 2$  K increases monotonically with  $H$ , but well below 2 K a weak peak in the MR is observed. The variation of the shape of the MR curve with  $x$  and with  $n_{\text{RT}}$  is discussed. The positive MR at low  $H$  is accompanied by an increase in  $|R|$ , but the behavior of  $R$  at high fields depends on  $x$  and on  $n_{\text{RT}}$ . A strong correlation between the MR and the magnetization of the Mn spins is found. This correlation indicates that the  $s$ - $d$  interaction is primarily responsible for the MR. Several competing mechanisms by which the  $s$ - $d$  interaction can produce large MR effects are discussed. However, the precise mechanisms which are responsible for the effects observed here have not been identified as yet.

## I. INTRODUCTION

The metal-insulator ( $M$ - $I$ ) transition in ordinary, nonmagnetic, semiconductors has been studied extensively for many years. Reviews of works prior to 1978 are given in Ref. 1. The important advances which were made since then, including the scaling theory of localization and the effects of electron-electron interactions, are summarized in Refs. 2 and 3. From studies of nonmagnetic semiconductors it is known that the low-temperature resistivity of samples which are near the  $M$ - $I$  transition is very sensitive to perturbations, e.g., to stress.<sup>4</sup> This sensitivity of the resistivity near the  $M$ - $I$  transition is also present in magnetic semiconductors (MS's) and in dilute magnetic semiconductors (DMS's). The unique feature of MS's and DMS's is the existence of a strong  $s$ - $d$  interaction<sup>5</sup> between the localized spins of the magnetic ions and the spins of electrons and holes near the band edges. This interaction allows one to perturb the carriers near the band edge by applying a magnetic field  $H$ , which aligns the localized spins. Dramatic changes in the resistivity as a function of  $H$  are therefore observed in these materials near the  $M$ - $I$  transition. Many of the works on the electrical-transport properties of MS's were carried out some time ago. These were reviewed by Nagaev<sup>6</sup> and by Leroux-Hugon.<sup>7</sup> An example of a more recent work on

the  $M$ - $I$  transition in a MS may be found in Ref. 8. Only a few studies of the electrical properties of DMS's were carried out thus far, most of them in the last few years. Examples are the works in Refs. 9 and 10. A general review of DMS's was given by Furdyna.<sup>11</sup>

In this paper we present the results of a systematic study of the magnetoresistance (MR) and Hall effect near the  $M$ - $I$  transition of the DMS  $\text{Cd}_{1-x}\text{Mn}_x\text{Se}$ . The study covers the Mn concentrations  $x=0.01$ ,  $0.05$ , and  $0.10$ . For each value of  $x$ , several  $n$ -type samples with different carrier concentrations were measured. Many of the results for  $x=0.01$ , and a few for  $x=0.05$ , were reported briefly earlier.<sup>12,13</sup> For this reason there is a greater emphasis in the present paper on the results for  $x=0.10$ . The series of samples for this Mn concentration covers a wide range of carrier concentrations  $n$ . It extends from below  $n_c$  to well above  $n_c$ , where  $n_c$  is the carrier concentration at the  $M$ - $I$  transition.

Experimental studies of the MR of  $\text{Cd}_{1-x}\text{Mn}_x\text{Se}$  have also been carried out recently by other groups. Dietl, Antoszewski, and Swierkowski studied several  $\text{Cd}_{0.95}\text{Mn}_{0.05}\text{Se}$  samples with  $n \ll n_c$ .<sup>14</sup> The MR of one  $\text{Cd}_{0.95}\text{Mn}_{0.05}\text{Se}$  sample, which was metallic but in the weakly localized regime, was measured by Sawicki *et al.* in fields up to 17 kOe.<sup>15</sup> Stankiewicz, von Molnar, and Giriat carried out magneto-transport measurements on in-

insulating samples of  $\text{Cd}_{0.6}\text{Mn}_{0.4}\text{Se}$ .<sup>16</sup> Strictly, the three investigations just referred to do not overlap with the present work because the combinations  $(x, n)$  in these studies are all outside the range which is covered here. Nevertheless, the qualitative features of the MR data reported by these groups are similar to our results. MR measurements in the parent compound CdSe are reported in Refs. 14, 15, and 17. The  $M$ - $I$  transition in CdSe is also discussed in Ref. 17.

The carrier concentration  $n_c$  at the  $M$ - $I$  transition is usually estimated from the Mott relation<sup>1</sup>

$$n_c \cong (0.26/a_H)^3, \quad (1)$$

where  $a_H$  is the effective Bohr radius for the donor. For  $n$ -type CdSe this equation gives  $n_c \cong 3 \times 10^{17} \text{ cm}^{-3}$ , which agrees (at least approximately) with the data in Ref. 17. The results which are reported below and in Ref. 16 indicate that in  $\text{Cd}_{1-x}\text{Mn}_x\text{Se}$ ,  $n_c$  increases with increasing  $x$ . Nevertheless, the value of  $n_c$  in the parent compound sets the order of magnitude of the carrier concentrations which are required for studying the  $M$ - $I$  transition in samples with  $x \leq 0.1$ . This is of practical importance because samples of  $\text{Cd}_{1-x}\text{Mn}_x\text{Se}$  which are not doped intentionally usually have carrier concentrations which are below  $1 \times 10^{17} \text{ cm}^{-3}$ . Thus, intentional doping is required in order to reach  $n_c$ . The development of techniques for controlled doping of the crystals<sup>18</sup> was a prerequisite for the present work.

There is strong evidence that the large MR effects which are reported here are caused primarily by the  $s$ - $d$  interaction. However, as yet there is no complete theoretical understanding of the detailed mechanisms by which the  $s$ - $d$  interaction produces these effects; some mechanisms are known but their relative contributions are not always known, nor is it certain that still other mechanisms are not involved. For this reason it is important to distinguish between (i) experimental facts and some inferences based on these facts, which are believed to be reliable, and (ii) theoretical conjectures concerning detailed mechanisms which may account for the data. The structure of the paper emphasizes this distinction. The experimental techniques are described in Sec. II. Experimental results, and inferences based on these results, are presented in Sec. III. Theoretical conjectures are discussed in Sec. IV.

## II. EXPERIMENTAL TECHNIQUES

### A. Samples

Electrical-transport measurements were carried out on  $n$ -type single-crystal samples of  $\text{Cd}_{1-x}\text{Mn}_x\text{Se}$ . These were obtained from boules grown by a modified Bridgman method. The desired carrier concentrations were achieved by adding controlled amounts of Ga into the melts from which the samples were grown, and by using two annealing procedures. First the entire boule was annealed. Then a thin slice, approximately 0.8 mm in thickness, was cut from the boule and was annealed in Cd vapor. A sample for electrical-transport measurements was then cut from the annealed slice. The crystal-growth and annealing pro-

TABLE I. Electrical properties of Ga-doped  $\text{Cd}_{1-x}\text{Mn}_x\text{Se}$  samples at zero magnetic field.<sup>a</sup>

Sample No.	$x$	Ga in melt ( $10^{17}$ atoms/cm <sup>3</sup> )	$n_{RT}$ ( $10^{17}$ cm <sup>-3</sup> )	$\rho_{RT}$ ( $10^{-2}$ $\Omega$ cm)	$\mu_{RT}$ (cm <sup>2</sup> /V s)	$n_{77K}$ ( $10^{17}$ cm <sup>-3</sup> )	$\rho_{77K}$ ( $10^{-2}$ $\Omega$ cm)	$\mu_{77K}$ (cm <sup>2</sup> /V s)	$n_{4.2K}$ ( $10^{17}$ cm <sup>-3</sup> )	$\rho_{4.2K}$ ( $10^{-1}$ $\Omega$ cm)	$\mu_{4.2K}$ (cm <sup>2</sup> /V s)
1-1	0.01	8	2.3	4.1	652	1.6	4.8	819	~0.8	2.5	~310
1-2	0.01	10	3.0	3.6	576	2.3	4.0	683	~2.4	1.0	~260
1-3	0.01	12	4.3	2.6	557	3.7	2.9	584	~4.2	0.43	~340
5-1	0.05	10	3.2	4.2	464	2.1	5.7	511	~2	2.1	~140
5-2	0.05	17	5.3	2.7	443	4.7	3.0	438	~4.9	0.44	~290
10-1	0.10	10	2.3	6.4	429	1.4	8.0	576	~0.16	55	~75
10-2	0.10	12	3.7	5.0	343	2.7	6.4	364	~1.5	3.8	~110
10-3	0.10	14	5.3	3.6	323	4.4	4.5	313	~4.4	1.0	~140
10-4A	0.10	19	6.0	2.7	379	5.5	3.4	331	~5.2	0.52	~235
10-4B	0.10	19	6.2	2.8	360	5.5	3.4	334	~5.4	0.50	~230
10-5	0.10	70	19	1.1	293	19	1.2	292	~18	0.12	~280

<sup>a</sup>Carrier concentration  $n = 1/|Re|$ , resistivity  $\rho$ , and Hall mobility  $\mu$  at room temperature ( $RT = 293 \pm 4$  K), 77 K, and 4.2 K. Values of  $n$  and  $\mu$  at 4.2 K are estimates based on extrapolation to  $H = 0$ . The concentration of Ga in the melt from which the sample was grown is also given.

cedures are described in detail in Ref. 18.

The samples in this paper are designated by two numbers separated by a dash. The first number indicates the Mn concentration  $x$ , in percent. The second number increases sequentially with increasing room-temperature carrier concentration  $n_{RT}$ . For example, sample No. 10-1 is the sample with the lowest carrier concentration among all the samples with  $x=0.10$ . In one case, two samples were cut from the same slice. These are samples Nos. 10-4A and 10-4B. All other samples were obtained from slices which originated from different boules.

Table I lists the Ga concentrations in the melts from which the various samples were grown. The values of  $n_{RT}$  are also given in this table. They range from  $2 \times 10^{17}$  to  $19 \times 10^{17} \text{ cm}^{-3}$ . The ratio between  $n_{RT}$  and the Ga concentration in the melt shows some variation, but is typically equal to 0.3. An analysis for the Ga concentration in the crystal (as distinguished from the concentration in the melt) was carried out only in one case, using atomic absorption.<sup>19</sup> This analysis was performed on a portion of the slice from which sample No. 10-5 was cut. The Ga concentration  $(4.5 \pm 0.5) \times 10^{18} \text{ atoms/cm}^3$  which was found should be compared with the Ga concentration  $7.0 \times 10^{18} \text{ atoms/cm}^3$  in the melt and with  $n_{RT} = 1.9 \times 10^{18} \text{ cm}^{-3}$ .

In many cases a comparison was made between the resistivity of the sample and the resistivity of the entire slice from which that sample was cut. Both resistivities were measured at room temperature. (The van der Pauw method was used for the slice.) The results always agreed to better than 10%, which was well within the combined experimental uncertainty. In addition, the resistivities and carrier concentrations of samples No. 10-4A and No. 10-4B, which were cut from the same slice, agreed to within several percents. These results are consistent with a reasonably uniform carrier concentration within a given slice. It is also shown in Ref. 18 that slices obtained from the same boule using the same annealing procedures have the same resistivities to within 10% or so.

As already stated, all samples which are included in this paper were grown and annealed using the procedure in Ref. 18. Not included are several samples with  $x=0.05$  which were obtained before the crystal-growth and annealing procedure was standardized. The results for these early samples were qualitatively similar to those reported below, but they indicate that the carrier concentration  $n_c$  at the  $M$ - $I$  transition depends on the crystal growth and annealing procedure. This dependence, at least in part, may be due to a change of  $n_c$  with compensation. The degree of compensation was not determined in the present work.

### B. Resistivity and Hall measurements

Resistivity and Hall measurements were made on bar-shaped samples with typical dimensions of  $7 \times 1.6 \times 0.8 \text{ mm}^3$ . Five thin copper leads (two for current and three for voltage) were attached to each sample using indium and an ultrasonic soldering iron. The contacts were Ohmic. Measurements were made with dc currents, which varied between  $1 \mu\text{A}$  and  $10 \text{ mA}$ , depending on the tem-

perature and on the sample. The proportionality between the measured voltage and the current was always checked, to ensure Ohmic behavior and the absence of self-heating.

The MR and Hall data were taken in fields up to 80 kOe, using Nb-Ti superconducting magnets. The magnetic field  $\mathbf{H}$  was always perpendicular to the direction of the current in the sample. The standard procedure of reversing the direction of  $\mathbf{H}$  was used to separate the resistive and Hall components of the voltage. The main source of uncertainty in the resistivity measurements was the finite size of the contacts, which made the distance between the two voltage probes uncertain to within 10% or so. Thus, the accuracy of the resistivity  $\rho$  was approximately 10%. However, changes of  $\rho$  as the function of  $H$  or temperature  $T$  were measured with a precision of 0.1%. Because the results for the Hall mobility  $\mu$  depend on  $\rho$ , the accuracy and precision for  $\mu$  were limited by those for  $\rho$ .

The voltage contacts in the Hall measurements consisted of one of the voltage contacts used in the resistivity measurements and another on the opposite side of the sample. A small unintentional offset between these two contacts, along the direction of the current, was always present. The resistive voltage component due to this offset was eliminated by using only the voltage component which was odd in  $H$ . However, because the field reversal was never perfect, there was some uncertainty in the Hall voltage. This uncertainty was significant at low  $H$  and low  $T$ , where the Hall voltage was small and the resistive voltage was sensitive to the magnitude of  $H$ . The total uncertainty in the Hall coefficient  $R$ , due to this and other sources, will be indicated in figures which show Hall data.

All the samples were measured in the temperature range 1.5–300 K. In addition, some of the samples were also measured between 0.3 and 1.5 K, or between 0.5 and 1.5 K. The measurements below 1.5 K were carried out with the samples immersed in liquid  $^3\text{He}$ .

## III. RESULTS

### A. Behavior at $H=0$

The resistivity  $\rho$ , carrier concentration  $n$ , and Hall mobility  $\mu$  at room temperature (RT) are given in Table I. Here, and throughout this paper,  $n$  is obtained from the Hall coefficient  $R$  using the relation  $n = 1/|Re|$ , where  $e$  is the electron's charge. As mentioned above, the values of  $\rho$  and  $\mu$  are subject to a typical uncertainty of 10%. Nevertheless, the results in Table I strongly suggest that the room-temperature mobility  $\mu_{RT}$  decreases with increasing  $x$ .

On cooling from room temperature to 200 K the resistivity of each of the samples decreases slightly. On further cooling,  $\rho$  goes through a broad minimum and then starts to increase with decreasing  $T$ . A typical example is the behavior of sample No. 10-2. For this sample  $\rho$  decreases from  $5.0 \times 10^{-2} \Omega \text{ cm}$  at room temperature to a minimum value of  $4.5 \times 10^{-2} \Omega \text{ cm}$  at 185 K. Below 185 K,  $\rho$  increases with decreasing  $T$ . The electrical properties of all the samples at 77 and 4.2 K are summarized in Table I. The values of  $n$  and  $\mu$  at 4.2 K are estimates based on extrapolations from finite  $H$  to  $H=0$ .

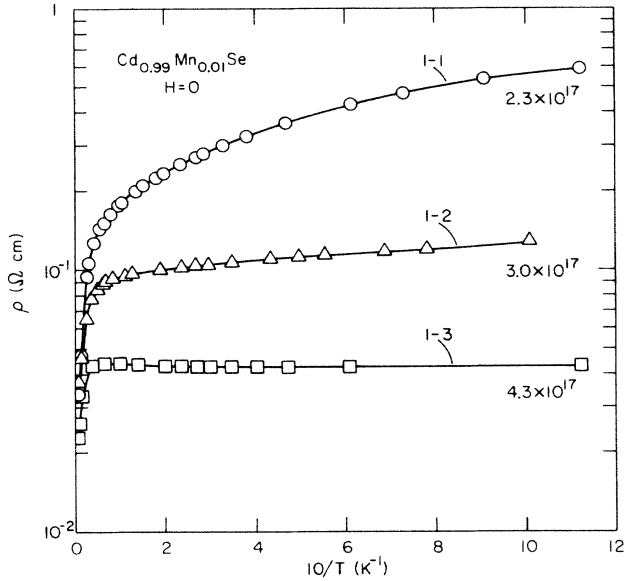


FIG. 1. Temperature dependence of the resistivity  $\rho$  at zero field for samples with  $x=0.01$ . The room-temperature carrier concentration  $n_{RT}$  for each sample (in electrons/cm<sup>3</sup>) is indicated.

The temperature variation of the zero-field resistivity at low temperatures is shown in Figs. 1–3. (The results for sample No. 10-4A are omitted in Fig. 3 because they are very close to those for sample No. 10-4B.) By definition, a sample is on the metallic or insulating side of the  $M-I$  transition depending on whether its resistivity at  $T=0$  is finite or infinite. In what follows we use the data in Figs. 1–3 to estimate the carrier concentration  $n_c$  at the  $M-I$  transition, for each value of  $x$ . These estimates are subject to some uncertainty because they involve extrapolations of data at relatively high temperatures to  $T=0$ .

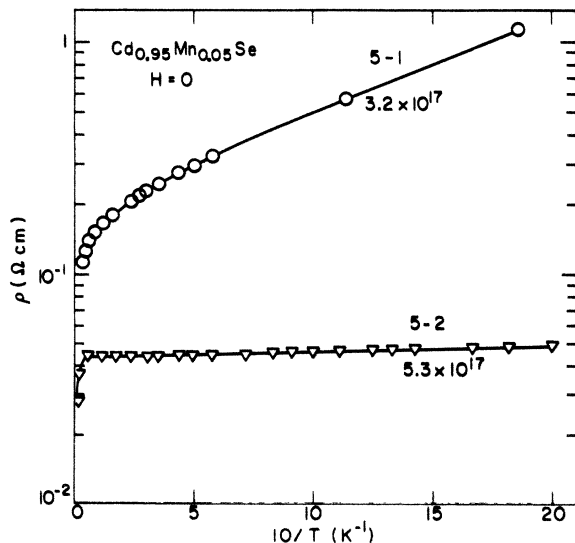


FIG. 2. Temperature dependence of the zero-field resistivity of samples with  $x=0.05$ . Values of  $n_{RT}$  are indicated.

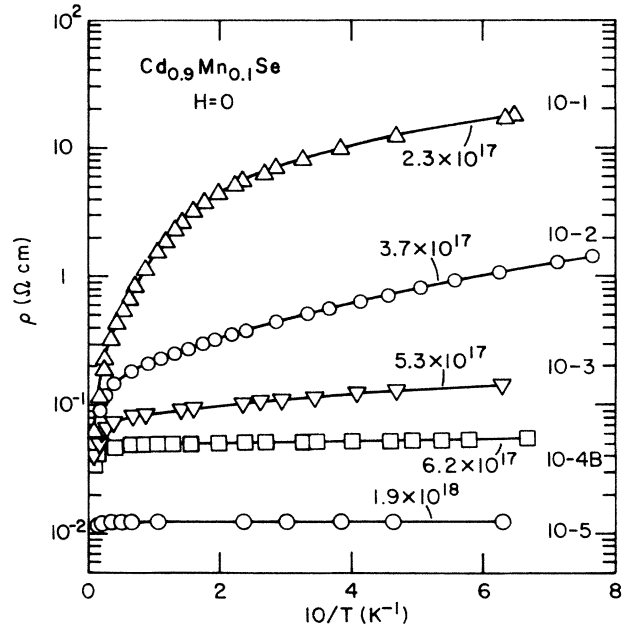


FIG. 3. Temperature dependence of the zero-field resistivity of samples with  $x=0.10$ . Values of  $n_{RT}$  are indicated.

Nevertheless, we believe that our main conclusion concerning the dependence of  $n_c$  on  $x$  is valid.

Consider first the results in Fig. 1 for  $x=0.01$ . For sample No. 1-3 the resistivity is very nearly independent of  $T$  at the lowest temperatures. Data down to 0.5 K for this sample (not shown) indicate that  $\rho$  increases by only 3% between 2 and 0.5 K. These results suggest that sample No. 1-3 is metallic, although the possibility that the sample is just on the insulating side of the  $M-I$  transition cannot be ruled out entirely. For sample No. 1-2,  $\rho$  increases by 25% between 4.2 and 1.0 K. This relatively small increase places the sample near the  $M-I$  transition. Sample No. 1-1 appears to be on the insulating side of the transition, but still fairly close to it. From these results and the values of  $n_{RT}$  we conclude that the estimate  $n_c \cong 3 \times 10^{17} \text{ cm}^{-3}$ , which was based on Eq. (1) and the parameters for  $x=0$ , is consistent with the behavior of the samples with  $x=0.01$ .

For  $x=0.10$  the estimate  $n_c \cong 3 \times 10^{17} \text{ cm}^{-3}$  is clearly too low, as can be seen from the behavior of sample No. 10-2 in Fig. 3. For this sample, with  $n_{RT} = 3.7 \times 10^{17} \text{ cm}^{-3}$ , the resistivity at low  $T$  is activated. Sample No. 10-3, with  $n_{RT} = 5.3 \times 10^{17} \text{ cm}^{-3}$ , still shows a small activation energy at low temperatures (a 42% increase in  $\rho$  between 4.2 and 1.6 K) and is probably on the insulating side of the  $M-I$  transition. Sample No. 10-4B, with  $n_{RT} = 6.2 \times 10^{17} \text{ cm}^{-3}$ , exhibits only an 8% increase in  $\rho$  between 4.2 and 1.5 K, which places this sample near the  $M-I$  transition. Sample No. 10-5 ( $n_{RT} = 1.9 \times 10^{18} \text{ cm}^{-3}$ ) is metallic; its resistivity changes by less than 0.1% between 15 and 1.6 K. On the basis of these results we estimate that  $n_c \cong 6 \times 10^{17} \text{ cm}^{-3}$  for  $x=0.10$ , which is roughly a factor of 2 higher than for  $x=0.01$ . For  $x=0.05$  the data in Fig. 2 suggest that  $n_c \cong 5 \times 10^{17} \text{ cm}^{-3}$ . Thus, we conclude that  $n_c$  increases with increasing  $x$ . This conclusion is consistent with the data in Ref.

16, which give  $n_c > 1.5 \times 10^{18} \text{ cm}^{-3}$  for  $x=0.4$ .

The zero-field resistivity of two samples with  $x=0.10$  was measured below 1.5 K. For sample No. 10-2,  $\rho$  increased by a factor of 26 between 4.2 and 0.50 K. In this temperature range,  $\log \rho$  was linear in  $1/T^{1/2}$ . (We note, however, that this  $T^{1/2}$  behavior was not found in sample No. 10-1 between 6 and 1.5 K.) For sample No. 10-4A,  $\rho$  increased by a factor of 1.7 between 4.2 and 0.33 K. Over this temperature range  $\log \rho$  was approximately linear in  $1/T$ .

A spin-glass behavior was reported for  $x=0.10$  at  $T < 0.5 \text{ K}$ .<sup>20</sup> We have therefore searched for hysteresis effects in the zero-field resistivity of sample No. 10-4A at 0.40 and 0.33 K. The zero-field resistivity was first measured after cooling in zero field, and was then remeasured after a field of 10 kOe was applied and was reduced back to zero. No difference was found.

## B. Magnetoresistance at $T \leq 4.2 \text{ K}$

### 1. General features

Typical examples of the magnetoresistance (MR) at low temperatures for samples with different  $x$  are shown in Fig. 4. For the sample with  $x=0.01$  the resistivity increases monotonically with increasing  $H$ . For the sample with  $x=0.05$  the resistivity first increases with increasing  $H$ , then goes through a maximum, and finally decreases. The MR of the sample with  $x=0.10$  is qualitatively similar to that for  $x=0.05$ , except that the decrease of  $\rho$  at high fields is more pronounced. For all three samples the MR is leveling off at the highest fields.

The magnitudes of the resistivity changes in Fig. 4 are specific to these samples at these temperatures. However, each of the curves in Fig. 4 has the qualitative features which are found in all samples with the same  $x$  at  $T \leq 4.2 \text{ K}$ . Specifically, the following characteristics are observed

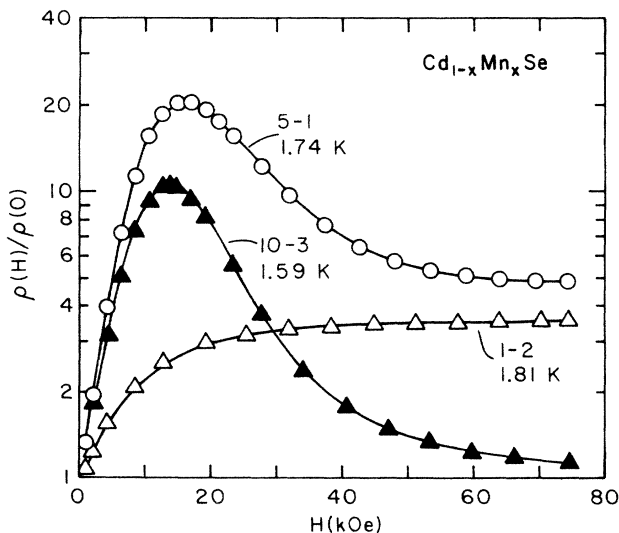


FIG. 4. Transverse magnetoresistance of sample No. 1-2 ( $x=0.01$ ,  $n_{RT}=3.0 \times 10^{17} \text{ cm}^{-3}$ ), sample No. 5-1 ( $x=0.05$ ,  $n_{RT}=3.2 \times 10^{17} \text{ cm}^{-3}$ ), and sample No. 10-3 ( $x=0.10$ ,  $n_{RT}=5.3 \times 10^{17} \text{ cm}^{-3}$ ).

in all samples in the fields below 80 kOe: (i) At low fields the MR is always positive; (ii) For samples with  $x=0.05$  and 0.10, the resistivity as a function of  $H$  goes through a maximum, and it then decreases at higher  $H$ . (iii) For samples with  $x=0.01$ , the resistivity at  $2 \leq T \leq 4.2 \text{ K}$  increases monotonically with increasing  $H$ , but at temperatures well below 2 K a slight decrease of  $\rho$  occurs at the highest fields. (iv) In all cases,  $\rho$  tends to level off at the highest fields.

### 2. Correlation between the MR and the magnetization

The observed MR is quite large; in several samples  $\rho$  changes by more than an order of magnitude. Such a large MR cannot be associated with the classical MR due to the Lorentz force. One reason is that the classical MR, which is of order  $(\mu H)^2$ , is far too small. For example, an analysis of the MR of sample No. 10-1 at 4.2 K (not shown) indicates that the maximum MR is 4 or 5 orders of magnitude larger than the classical MR. For sample No. 5-2 at 4.2 K the MR at 4.2 K (Fig. 5) is 2–3 orders of magnitude larger than  $(\mu H)^2$ . Another argument is that for all samples the MR at room temperature or at 77 K is orders of magnitude smaller than at 4.2 K, even though the mobilities at RT and at 77 K are higher than at 4.2 K. In what follows we present evidence that the MR is governed primarily by the magnetization  $M$ . Later on, in Sec. IV, it will be shown that the connection between the MR and the magnetization indicates that the MR is primarily caused by the  $s$ - $d$  interaction between the Mn spins and the spins of the conduction electrons.

Three features of the MR correlate well with the behavior of the magnetization: (i) Measurements of the magnetization<sup>21</sup> indicate that the slope  $dM/dH$  at low fields increases at  $T$  decreases. The same behavior is also found in the MR, i.e., the increase of the resistivity at low  $H$  is steeper at lower temperatures, for all samples. This is illustrated by the data in Fig. 5. (ii) At the highest

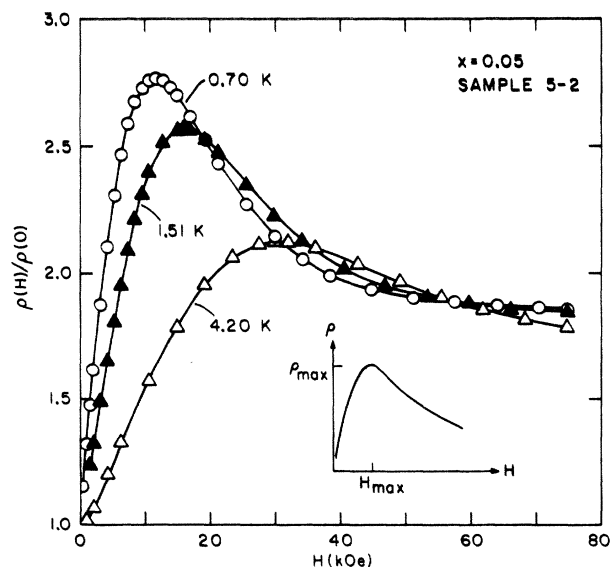


FIG. 5. Transverse magnetoresistance of sample No. 5-2. The definitions of  $H_{\max}$  and  $\rho_{\max}$  are indicated in the inset.

fields used in the present experiments the magnetization at low temperatures varies only slowly with  $H$ .<sup>21</sup> A similar behavior is also observed in the resistivity, i.e., the slope  $d\rho/dH$  is relatively small at the highest fields. This is illustrated by the data in Figs. 4 and 5. (iii) The MR of samples with  $x=0.05$  and  $0.10$ , as a function of  $H$ , exhibits a well-defined maximum at  $H_{\max}$  (Figs. 4 and 5). It will be shown later that for a given sample the magnetization at  $H_{\max}$  is nearly independent of  $T$ . This is in contrast with the appreciable temperature dependence of  $H_{\max}$ . Thus, there is a strong correlation between the MR and the magnetization.

### 3. Magnetoresistance versus magnetization

Because the MR appears to be governed by the magnetization, it seems appropriate to plot the MR as a function of  $M$ . To produce such plots we use a phenomenological equation for  $M$ , introduced by Gaj *et al.*,<sup>22</sup> namely,

$$M = M_s B_{5/2}(5\mu_B H/k(T + T_0)), \quad (2)$$

where  $B_{5/2}$  is the Brillouin function for spin  $S = \frac{5}{2}$ ,  $k$  is the Boltzmann constant,  $\mu_B$  is the Bohr magneton, and  $M_s$  and  $T_0$  are phenomenological parameters which depend on  $x$  but which are nearly temperature independent at  $T \leq 4.2$  K. Tests carried out on insulating  $\text{Cd}_{1-x}\text{Mn}_x\text{Se}$  samples with  $x=0.05$  and  $0.10$  show that Eq. (2) gives a good description of the magnetization when  $1.5 \leq T \leq 4.2$  K and  $H \leq 80$  kOe.<sup>21</sup> Moreover, the parameters  $M_s$  and  $T_0$  vary only slightly between 4.2 and 1.5 K. In what follows we assume that Eq. (2) is obeyed at all temperatures  $T \leq 4.2$  K, with parameters  $M_s$  and  $T_0$  which depend only on  $x$  but not on  $T$  or  $n_{\text{RT}}$ . Although these assumptions hold only approximately, we expect that any errors in the plots of the MR versus  $M$  will be too small to affect the conclusions.

The parameter  $M_s$ , which is called the technical saturation value, was the subject of recent studies.<sup>23</sup> For present purposes, however,  $M_s$  is simply a constant for a given  $x$ . The value of this constant does not enter in plots of the MR as a function of the ratio  $M/M_s$ . Such plots were first introduced by Stankiewicz *et al.*<sup>16</sup> To evaluate  $M/M_s$  from Eq. (2) one needs to know  $T_0$ . Based on the results in Table I of Ref. 21 we set  $T_0 = 1.6$  K for

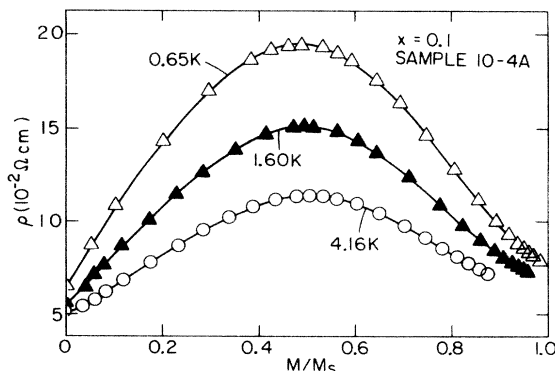


FIG. 6. Transverse magnetoresistance of sample No. 10-4A as a function of reduced magnetization  $M/M_s$ .

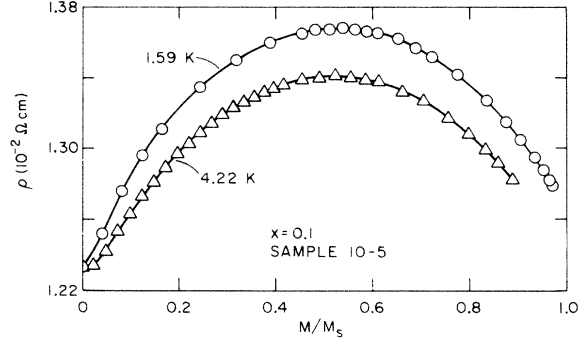


FIG. 7. Transverse magnetoresistance of sample No. 10-5 as a function of  $M/M_s$ .

$x=0.05$ , and  $T_0 = 2.4$  K for  $x=0.10$ . Plots of the resistivity versus  $M/M_s$  for three samples with  $x=0.10$  are shown in Figs. 6–8.

Figures 6–8 indicate that for each sample the resistivity maxima at all temperatures occur at approximately the same value of  $M/M_s$ . All other samples with  $x=0.05$  and  $0.10$  exhibit a similar behavior. This is shown explicitly in Fig. 9. (The results for sample No. 10-4B are not shown because they are very close to those for sample No. 10-4A.) The value of  $M/M_s$  at the resistivity maximum will be called  $(M/M_s)_{\max}$ . For most samples the variation of  $(M/M_s)_{\max}$  with  $T$  is no more than a few percents. The largest change is for sample No. 10-2, in which a 15% decrease occurs between 4.16 and 0.65 K. This 15% change is still very small compared with the change of  $H_{\max}$  for this sample, from 21.9 kOe at 4.16 K to 8.4 kOe at 0.65 K.

The dependence of  $(M/M_s)_{\max}$  on the room-temperature carrier concentration  $n_{\text{RT}}$  is given implicitly by the results in Fig. 9 and the values of  $n_{\text{RT}}$  in Table I. For  $x=0.10$  it is clear that at a given temperature  $(M/M_s)_{\max}$  increases with  $n_{\text{RT}}$ . The results for the two

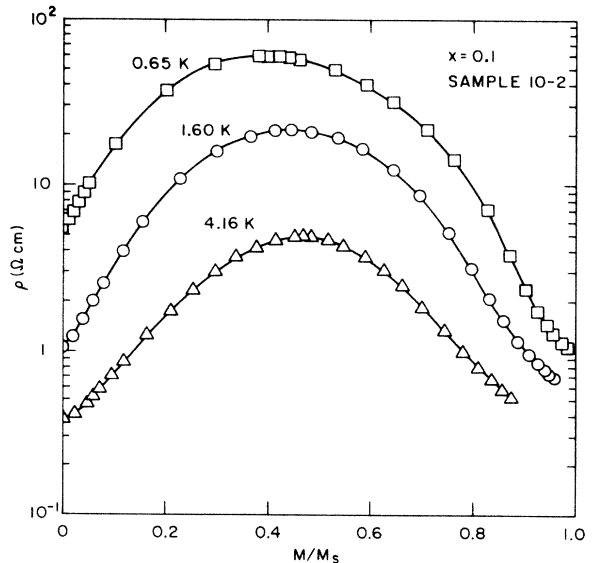


FIG. 8. Transverse magnetoresistance of sample No. 10-2, plotted as a function of  $M/M_s$ .

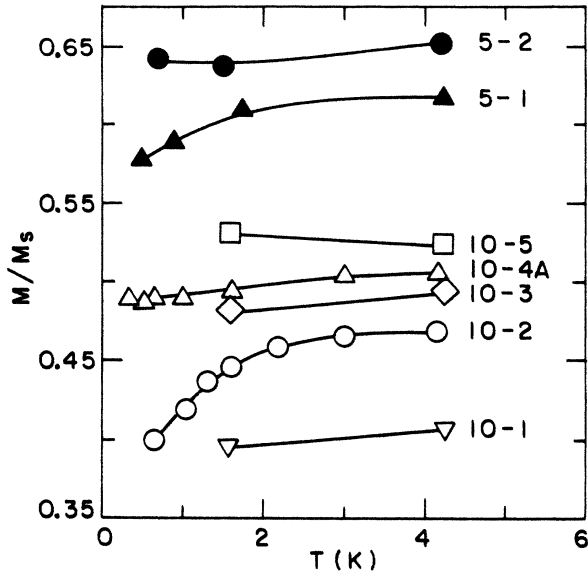


FIG. 9. Reduced magnetization  $M/M_s$  at  $H_{\max}$  for various samples at various temperatures.

samples with  $x=0.05$  are also consistent with this trend. Note, however, that the increase of  $(M/M_s)_{\max}$  with  $n_{RT}$  is fairly weak. For example, the carrier concentration of sample No. 10-5 is 3 times that of sample No. 10-4A, but  $(M/M_s)_{\max}$  is larger by only several percents.

Figure 9 also shows that for samples with comparable values of  $n_{RT}$ , or comparable values of  $n_{RT}/n_c$ , the values of  $(M/M_s)_{\max}$  are larger for  $x=0.05$  than for 0.10. Also, for samples with  $x=0.01$  (in the low-temperature region where the MR has a maximum) the values of  $(M/M_s)_{\max}$  are larger than for comparable samples with  $x=0.05$ .

#### 4. Maximum MR and the shape of the MR curve

The following brief comments summarize some features of the MR curve. In samples with  $x=0.05$  and 0.10 the resistivity versus  $H$  (or  $M$ ) reached a maximum value  $\rho_{\max}$  (Fig. 5). For all such samples the ratio  $\rho_{\max}/\rho(0)$  increased with decreasing  $T$  in the temperature region  $1.5 \leq T \leq 4.2$  K. However, some of the samples which were studied below 1.5 K showed a decrease of  $\rho_{\max}/\rho(0)$  at the lowest temperatures. This decrease was particularly pronounced in sample No. 10-2 (Fig. 8). In this sample  $\rho_{\max}/\rho(0)$  increased from 12.9 at 4.16 K to 20.1 at 1.60 K, but it then decreased to 10.9 at 0.65 K.

There are insufficient data to make definitive statements concerning the correlation between the magnitude of the MR and the carrier concentration  $n_{RT}$ . However, the data for sample No. 10-5 suggest that samples which are well on the metallic side of the  $M-I$  transition ( $n_{RT} \gg n_c$ ) have a much smaller MR than samples which are slightly on the insulating side of the transition.

In samples with  $x=0.05$  and 0.10 the shape of the MR curve is determined, in part, by the magnitude of the decrease of  $\rho$  in fields above  $H_{\max}$  in relation to the magnitude of the increase below  $H_{\max}$ . A comparison of dif-

ferent samples indicates that for similar values of  $n_{RT}/n_c$  and  $T$  the decrease of  $\rho$  above  $H_{\max}$  (relative to the increase below  $H_{\max}$ ) is more pronounced for  $x=0.10$  than for 0.05. This trend continues as  $x$  changes from  $x=0.05$  to 0.01; the resistivity of samples with  $x=0.01$  and  $n_{RT} \cong n_c$  does not decrease at high fields when  $T \geq 2$  K, and shows only a slight decrease when  $T \ll 2$  K. This dependence of the shape of the MR curve on  $x$  is well illustrated by the results in Fig. 4. For samples with a constant Mn concentration ( $x=0.10$  or 0.05) a decrease in the carrier concentration  $n_{RT}$  results in a stronger decrease of  $\rho$  above  $H_{\max}$ , relative to the increase below  $H_{\max}$ . This is illustrated by the results for sample No. 10-2 at 1.60 K (Fig. 8) as compared with those for sample No. 10-5 at 1.59 K (Fig. 7).

#### 5. MR at low fields

Detailed measurements of the MR at low fields were carried out on samples No. 10-2 and No. 10-4A. The results, as a function of  $H^2$ , are presented in Figs. 10 and 11. These data show, once again, that the initial rise of the resistivity becomes steeper with decreasing  $T$ . Because the MR is an even function of  $H$ , one expects it to be proportional to  $H^2$  at low  $H$ . This prediction is clearly obeyed at the higher temperatures, but at the lowest temperatures the MR versus  $H^2$  shows a marked curvature even in fields below 1 kOe. Presumably, the field range over which the MR is proportional to  $H^2$  is quite narrow at these low temperatures.

#### C. Hall measurements at low $T$

Hall measurements were carried out on all samples at 4.2 K. For samples with  $x=0.01$ , Hall data were also taken between 1.6 and 1.8 K. The Hall data were always analyzed on the assumption that the anomalous Hall term was negligible compared to the ordinary Hall term. This assumption can be justified on both theoretical and experi-

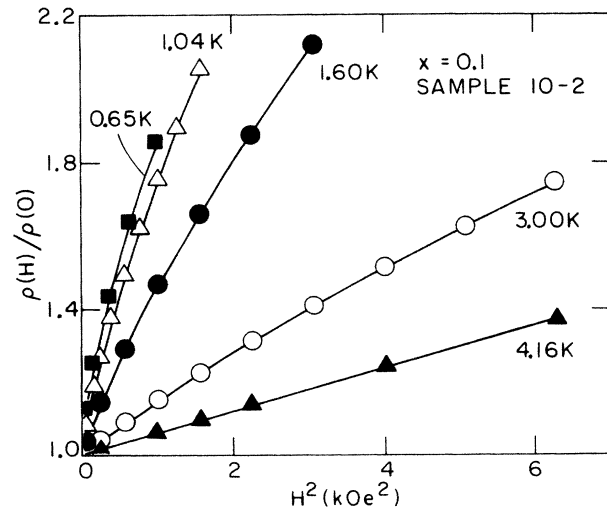


FIG. 10. Transverse magnetoresistance of sample No. 10-2 at low fields.

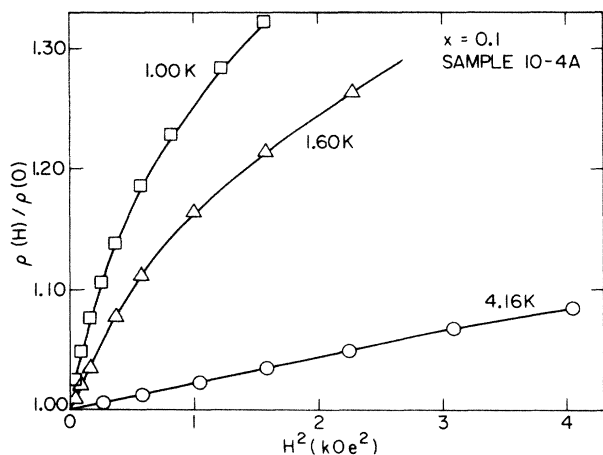


FIG. 11. Transverse magnetoresistance of sample No. 10-4A at low fields.

mental grounds. First, the anomalous Hall effect is caused by a spin-orbit interaction, which is negligible in the present conduction band (*s* band). Second, the anomalous Hall voltage is proportional to  $M$ , but the susceptibility of the present samples is orders of magnitude smaller than those in ferromagnetic metals and ferromagnetic semiconductors. To evaluate the anomalous Hall term experimentally we focused on cases in which the resistivity at the highest fields was nearly constant. It is reasonable to assume that in such cases the carrier concentration at these high fields is nearly constant. The ordinary Hall voltage should then be nearly proportional to  $H$ , whereas the anomalous Hall voltage should be nearly constant because the magnetization at these high fields varies only slowly with  $H$ . The fact that the observed Hall voltage was nearly proportional to  $H$  was therefore taken to mean that the anomalous Hall term was small compared with the ordinary term. A good example of a

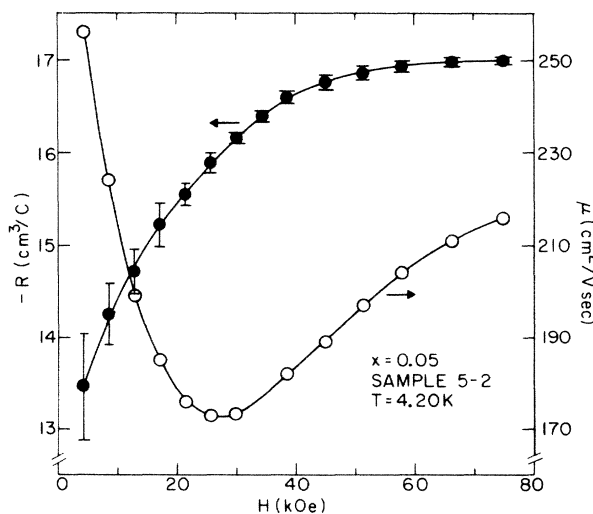


FIG. 12. Magnetic field dependence of the Hall coefficient  $R$  (solid circles) and Hall mobility  $\mu$  (open circles) for sample No. 5-2 at 4.20 K.

Hall voltage which is proportional to  $H$  is provided by the results in Fig. 3 of Ref. 12. In this figure, the Hall coefficient  $R$  (proportional to the ratio between the Hall voltage and  $H$ ) is nearly constant between 40 and 70 kOe when  $T=1.63$  K. A similar behavior is suggested by the high-field results in Fig. 12, and by the high-field results for sample No. 10-5 (not shown).

Some of the Hall data for  $x=0.01$  were presented earlier.<sup>12</sup> Examples of results for samples with  $x=0.05$  and  $0.10$  are shown in Figs. 12 and 13. The Hall mobility  $\mu = |R/\rho|$  is also shown in these figures. Because  $\rho$  is measured with high precision, the precision for  $\mu$  (in percents) is the same as for  $R$ . The resistivity data which correspond to Fig. 12 are shown in Fig. 5. The resistivity data which correspond to Fig. 13 are not shown, but are very similar to the data for sample No. 10-4A in Fig. 6. The fields at the mobility minima in Figs. 12 and 13 are slightly lower than the fields at the corresponding resistivity maxima.

In discussing the Hall data we distinguish between the field region where  $\rho$  increases with  $H$ , and the region  $H > H_{\max}$  where the resistivity for  $x=0.05$  and  $0.10$  decreases with increasing  $H$ . For fields where  $\rho$  increases with  $H$ , the magnitude of  $R$  also increases with  $H$ , in all cases. At the same time the Hall mobility  $\mu$  decreases with increasing  $H$ , except in fields just below the resistivity maximum.

The behavior of the Hall coefficient in fields above  $H_{\max}$  depends on both the Mn concentration  $x$  and the carrier concentration  $n_{RT}$ . Consider first the two samples with  $x=0.05$ . In sample No. 5-1, the Hall coefficient in fields above  $H_{\max}$  decreases slightly with increasing  $H$ , but the major cause for the decrease in  $\rho$  is the increase of  $\mu$ . In sample No. 5-2, which has a higher carrier concentration and which is near the  $M$ - $I$  transition,  $|R|$  increases monotonically with  $H$  even in fields above  $H_{\max}$ . Thus, the decrease of  $\rho$  above  $H_{\max}$  is solely due to an increase of  $\mu$ . This is shown in Fig. 12.

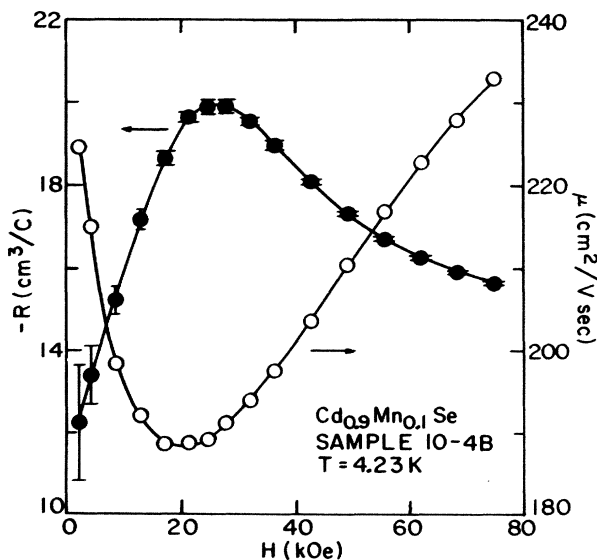


FIG. 13. Magnetic field dependence of  $R$  (solid circles) and  $\mu$  (open circles) for sample No. 10-4B at 4.23 K.

In those samples with  $x=0.10$  which are on the insulating side of the  $M$ - $I$  transition or near the  $M$ - $I$  transition, the decrease of  $\rho$  above  $H_{\max}$  is due to both a decrease of  $|R|$  and an increase of  $\mu$ . The two contributions are comparable. This is illustrated by the results in Fig. 13. However, in sample No. 10-5, which is well on the metallic side of the  $M$ - $I$  transition,  $|R|$  increases monotonically with  $H$  and the decrease of  $\rho$  above  $H_{\max}$  is solely due to an increase of  $\mu$ . This behavior is qualitatively similar to that of sample No. 5-2 in Fig. 12.

#### IV. DISCUSSION

A coherent theoretical picture which accounts for the preceding experimental results is not available at present. The picture which exists consists of (i) experimental evidence connecting the observed MR with the  $s$ - $d$  interaction, (ii) some general theoretical results concerning the influence of the  $s$ - $d$  interaction on electrons near the bottom of the conduction band, and (iii) several proposed mechanisms which can lead to a large MR. These three topics are discussed below, after a brief comment concerning  $n_c$ .

As pointed out in Sec. III, there is a strong evidence that the carrier concentration  $n_c$  at the  $M$ - $I$  transition increases with  $x$ . Two possible causes for this dependence are the slow increase of the electron effective mass  $m^*$  with  $x$ ,<sup>24</sup> and the increased scattering due to the presence of Mn ions. The increase of  $m^*$  leads to a decrease of the effective Bohr radius  $a_H$  which, in turn, leads to an increase of  $n_c$  [cf. Eq. (1)]. The presence of Mn ions should lead to scattering by alloy potential fluctuations, and also to some magnetic scattering at low temperatures. The increase in scattering enhances localization and it should, therefore, increase  $n_c$ .

##### A. Spin splitting and spin scattering

The carrier concentrations of our samples are sufficiently high that the mobilities at 4.2 K are of order  $10^2$   $\text{cm}^2/\text{V sec}$ . This strongly suggests that the low-temperature conduction is by states which are either above the mobility edge or not far below it. There are basically two routes by which the  $s$ - $d$  interaction can affect the resistivity in this case: changes of the energy levels near the bottom of the conduction band, and scattering of electrons by Mn ions.

##### 1. Spin splitting

In the presence of a magnetic field the  $s$ - $d$  interaction leads to a spin splitting of the conduction band. This splitting is much larger than that due to the direct action of the magnetic field on the electron's spin. To a good approximation the spin splitting  $\delta$  is proportional to  $M$ .<sup>11</sup> Using the results of Refs. 21 and 23 it is easy to show that in  $\text{Cd}_{1-x}\text{Mn}_x\text{Se}$ ,

$$\delta = \delta_x M / M_s, \quad (3)$$

where  $\delta_x = 5.7$  meV for  $x=0.01$ , 19 meV for  $x=0.05$ , and 26 meV for  $x=0.10$ . These values for  $\delta_x$  also agree with the data in Ref. 25 to within several percents. For

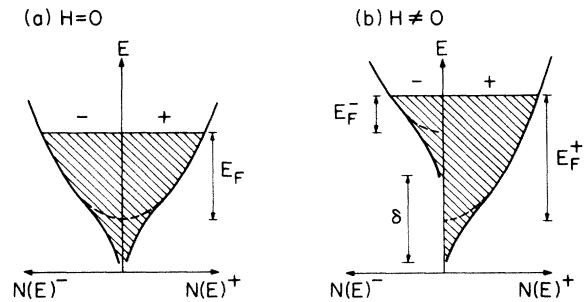


FIG. 14. Schematic showing the density of states  $N(E)$  as a function of energy  $E$  for the conduction band at  $H=0$  and  $H\neq 0$ . The two spin subbands are designated by (+) and (-). Shaded areas are regions occupied by electrons at low  $T$ .  $\delta$  is the spin splitting, and  $E_F$  is the Fermi energy measured from the bottom of the parabolic portion of the band (or subband).

$x \leq 0.1$  the parameter  $\delta_x$  is approximately equal to the spin splitting which is reached near 80 kOe when  $T \leq 4$  K.

The conduction-band splitting leads to a redistribution of electrons between the two spin subbands.<sup>26</sup> This is shown schematically in Fig. 14. To obtain a rough estimate of the energy scale in this figure, we use the effective mass  $m^* = 0.13m_0$  in the parent compound and assume that there are  $3 \times 10^{17}$  electrons/ $\text{cm}^3$  in the parabolic portion of the band at  $H=0$ . This leads to a Fermi energy  $E_F = 13$  meV at  $H=0$ , measured relative to the bottom of the parabolic portion of the band. Because the values of  $\delta_x$  are comparable to  $E_F$ , a substantial electron redistribution is expected when  $M$  approaches  $M_s$  at the highest fields. Even for the sample with the highest electron concentration ( $n_{\text{RT}} = 1.9 \times 10^{18}$   $\text{cm}^{-3}$ ,  $x=0.10$ ) an appreciable electron transfer between the subbands is expected from the estimate  $\delta_x/E_F = 0.6$ . As Fig. 14 indicates, the electron redistribution raises the Fermi energy  $E_F^+$  in the majority-spin subband, and lowers  $E_F^-$  in the other subband.

The density of states  $N(E)$  which is sketched in Fig. 14 is probably appropriate for samples which are well on the metallic side of the transition. Near the  $M$ - $I$  transition the band tail may have a different shape, and the Fermi energy is probably lower.<sup>27</sup> Nevertheless, the conclusion that a substantial electron redistribution occurs at high fields should remain valid. Another simplification in Fig. 14 is the implicit assumption that the density of states in a given subband is independent of  $\delta$ . Actually, some of the effects discussed below (e.g., the change in the screening radius) should affect the shape of the band tail.<sup>28</sup>

##### 2. Scattering by Mn spins

The  $s$ - $d$  interaction leads to a scattering of electrons by Mn spins. Two types of such scattering are known: spin-disorder scattering by Mn spins which are not near donors or acceptors, and coherent scattering from spin clusters associated with bound magnetic polarons (or similar entities) near donors or acceptors.

Spin-disorder scattering in the context of magnetic

semiconductors was discussed by Haas,<sup>29</sup> among others. The MR associated with this type of scattering is negative.<sup>26</sup> However, estimates for  $\text{Cd}_{1-x}\text{Mn}_x\text{Se}$  samples which are similar to those used here suggest that spin-disorder scattering is too weak to be of importance.<sup>15,30,31</sup>

Coherent magnetic scattering from ferromagnetic spin clusters associated with bound magnetic polarons (BMP's) is in some cases stronger than spin-disorder scattering.<sup>32</sup> Coherent scattering is most effective when the ferromagnetic alignment within the cluster, compared to the alignment outside the cluster, is appreciable. The latter condition is not satisfied for the usual BMP's in  $\text{Cd}_{1-x}\text{Mn}_x\text{Se}$ , i.e., for BMP's which are associated with shallow hydrogenic donors.<sup>33</sup> The reasons why the ferromagnetic alignment in these BMP's is very small are (i) a relatively large effective Bohr radius  $a_H$ , and (ii) a relatively weak magnetic susceptibility.<sup>21</sup> A very small ferromagnetic alignment is also expected for BMP's associated with weakly localized states which exist in samples near the  $M$ - $I$  transition. On the other hand, it is possible that our samples also contain some deep donors which are not ionized. Near such donors a stronger ferromagnetic spin alignment is expected, because the effective Bohr radius is smaller. This might lead to an appreciable coherent magnetic scattering. This scattering should be governed by the difference between the ferromagnetic order inside and outside the BMP, and it should, therefore, decrease as the spins outside the BMP are aligned by a magnetic field. Thus, a negative MR is expected.

### 3. Dominant role of the $s$ - $d$ interaction

The spin-splitting  $\delta$  is directly related to  $M$ . The MR associated with magnetic scattering is also expected to be governed by parameters which are related to  $M$ , e.g., the difference between the magnetization inside and outside the BMP should depend on the differential susceptibility  $\partial M/\partial H$ .<sup>21</sup> Thus, the observed strong correlation between the MR and  $M$  is a strong evidence that the  $s$ - $d$  interaction is the dominant cause for the MR.

#### B. Specific MR mechanisms

The observed MR is probably the result of several competing mechanisms, some giving a positive MR and others a negative MR. The negative MR associated with scattering from BMP's was already mentioned. Several other known mechanisms are listed below.

##### 1. Increase of the Thomas-Fermi screening radius

The scattering due to ionized impurities depends, in part, on the screening of the Coulomb potential of these impurities. In the Thomas-Fermi approximation the screening radius  $r_s$  is a function of the density-of-states  $N(E)$  at the Fermi energy  $E_F$ , summed over both spin subbands. As the conduction band splits, the redistribution of electrons between the two subbands produces a change of  $N(E)$  at  $E_F$ . For a parabolic band the spin splitting leads to an increase of  $r_s$ .<sup>26,34</sup> The maximum increase, for a complete transfer of electrons to the majority-spin subband, is by a factor of  $2^{1/3}$ . The increase

of  $r_s$  implies a weaker screening, and hence a stronger scattering. This should raise the mobility edge  $E_c$ . In addition, the density of states at the band tail should change, i.e., a larger number of electrons will be accommodated in the tail.<sup>28</sup> Both effects should lead to a positive MR.<sup>12</sup> However, theoretical estimates by Gan and Lee suggest that the increase of  $r_s$  is too weak to account for the large positive MR observed here.<sup>31</sup> A similar conclusion was also obtained by Stankiewicz *et al.* from an analysis of their data.<sup>16</sup> They therefore suggested that other mechanisms must also be important.

It may be of interest to note that the positive MR which accompanies the increase of  $r_s$  also follows from Mott's early heuristic derivation of Eq. (1) for  $n_c$ .<sup>35</sup> This derivation was based on the criterion  $r_s \sim a_H$  at the  $M$ - $I$  transition. When the same criterion is applied to the case in which the conduction band splits, it leads to an increase of  $n_c$ . For a complete transfer of electrons to the majority-spin subband,  $n_c$  increases by a factor of 4.<sup>36</sup> In a sample which is near the  $M$ - $I$  transition, the increase of  $n_c$  with increasing  $H$  should result in a positive MR at low temperatures.

#### 2. Change of the Fermi energy

Consider Fig. 14. As  $\delta$  increases, the Fermi energy  $E_F^+$  in the majority-spin subband rises relative to the bottom of the parabolic portion of the subband. The opposite is true for  $E_F^-$  in the minority-spin subband. The conductivity due to each subband depends on the difference  $E_F^\pm - E_C^\pm$  between the Fermi energy and the mobility edge for that subband, and is affected by the change in  $E_F^\pm$ . When the contributions of both subbands are added, and the changes in  $E_C^\pm$  are ignored, the net result is a negative MR.<sup>37</sup> Its magnitude can be appreciable, particularly on the insulating side of the  $M$ - $I$  transition.

#### 3. Effects of electron-electron exchange and correlation

The scattering of an electron from a screened charged impurity depends on the spin of the scattered electron and the net spin of the screening electrons. This is a consequence of exchange and correlation effects between electrons. If the screening electrons have a net  $+$  spin then the scattering of a  $+$  spin electron will be stronger than that of a  $-$  spin electron. Thus, in the presence of a magnetic field, which leads to a net spin polarization of both the scattered and screening electrons, the mobility for the minority-spin subband will be higher than that for the majority-spin subband. The consequences of exchange and correlation effects in the present context were considered recently by Gan and Lee.<sup>31</sup> An earlier treatment for the case of a ferromagnetic metal was given by Kim and Schwartz.<sup>38</sup> The  $H$ -induced shifts of the mobility edges  $E_C^\pm$  due to exchange-correlation effects can be much larger than the change caused by the variation of the Thomas-Fermi screening radius  $r_s$ . Thus, a much larger MR can occur. The sign of the MR at low  $H$  depends on the choice of parameters.

#### 4. Combined Coulomb and $s$ - $d$ scattering

In magnetic and semimagnetic semiconductors the scattering from ionized impurities is not always solely due to the Coulomb potential. Specifically, in the paramagnetic phase and when  $H \neq 0$  the screening electron cloud has a net  $s$ -spin polarization. This leads to an excess polarization of the  $d$  spins (Mn spins) in the vicinity of the impurity, relative to the polarization far away from the impurity. The complex consisting of the ionized impurity, the screening electron cloud, and the local excess magnetization of the Mn spins is physically similar to a BMP (or "localized ferrom" in Nagaev's terminology<sup>6</sup>). The scattering from this complex involves, therefore, both the Coulomb potential and the  $s$ - $d$  potential due to the excess polarization of the Mn spins. This problem is discussed in Ref. 6(b). The MR in the paramagnetic phase is discussed in Ref. 6(c) and in Ref. 39. Estimates based on these results suggest, however, that the contribution of the  $s$ - $d$  scattering potential to the MR is small in the present case. This agrees with the following intuitive argument. The excess Mn-spin polarization near an ionized impurity should be comparable to or smaller than the excess Mn-spin polarization in a BMP associated with a neutral hydrogenic donor. The latter excess polarization is very small in the present case, as already noted.

#### 5. Quantum corrections to the conductivity

Sawicki *et al.* measured the MR of a sample which was in the so-called weakly localized regime (WLR).<sup>15</sup> To interpret these data, they used expressions for quantum corrections to the conductivity in the WLR, but modified them to take into account the spin splitting of the conduction band.

#### C. Conclusion

The results in Sec. III, and those in Refs. 12–16, give a reasonably clear experimental picture of the behavior of the MR near the  $M$ - $I$  transition of  $\text{Cd}_{1-x}\text{Mn}_x\text{Se}$ . The theoretical picture, on the other hand, is still unsatisfactory. Although some MR mechanisms are known, their relative contributions are not always known. Nor is it clear that still other mechanisms are not important. For example, the decrease of  $\rho$  in high fields, for samples with  $x = 0.05$  and  $0.10$ , might be primarily due to (i) a decrease of scattering from BMP's associated with deep donors, or (ii) to changes in the Fermi energies  $E_F^\pm$ , or (iii) to still another (yet unidentified) mechanism. Our understanding of the  $H$ -dependence of the Hall coefficient is even less satisfactory, although it is clear that conduction in two subbands with different mobilities has an effect on  $R$ . Thus, the main challenge at present seems to be in the theoretical area.

#### ACKNOWLEDGMENTS

We are grateful to P. A. Lee and Z. Gan for useful discussions, to K. P. Martin and J. S. Brooks for their collaboration in the early phases of this work, to W. Bindilatti for assistance in some of the measurements, and to P. A. Wolff for encouragement. The work at the Francis Bitter National Magnet Laboratory was supported by the National Science Foundation under Contracts No. DMR-82-11416 and No. DMR-85-04366, and by the U.S. Office of Naval Research Contract No. N00014-81-K-0654. The work at Brown University was supported by the National Science Foundation Solid State Chemistry Grant No. DMR-86-01345. Crystal-growth facilities were provided by Brown University's Materials Research Laboratory, which is supported by the National Science Foundation. The work at the University of São Paulo was supported by Financiadora de Estudos e Projetos (FINEP). Additional support was provided by a joint grant from the U.S. National Science Foundation and the Brazilian Conselho Nacional de Desenvolvimento Científico e Tecnológico (CNPq).

<sup>1</sup>The Metal Non-Metal Transition in Disordered Systems, Proceedings of the Nineteenth Scottish Universities Summer School in Physics, St. Andrews, 1978, edited by L. R. Friedman and D. P. Tunstall (Scottish Universities Summer School in Physics, Edinburgh, 1978).

<sup>2</sup>B. I. Shklovskii and A. L. Efros, *Electronic Properties of Doped Semiconductors* (Springer, Berlin, 1984).

<sup>3</sup>P. A. Lee and T. V. Ramakrishnan, *Rev. Mod. Phys.* **57**, 287 (1985).

<sup>4</sup>M. A. Paalanen, T. F. Rosenbaum, G. A. Thomas, and R. N. Bhatt, *Phys. Rev. Lett.* **48**, 1284 (1982).

<sup>5</sup>We use the term  $s$ - $d$  interaction even though the localized spins are not always associated with  $d$  electrons, and the carriers near the band edges are not always  $s$ -like.

<sup>6</sup>(a) E. L. Nagaev, *Usp. Fiz. Nauk* **117**, 437 (1975) [*Sov. Phys.—Usp.* **18**, 863 (1976)]; E. L. Nagaev, *Physics of Magnetic Semiconductors* (Mir, Moscow, 1983), specifically (b) Chap. 7, (c) p. 344ff.

<sup>7</sup>P. Leroux-Hugon, *J. Magn. Magn. Mater.* **3**, 165 (1976).

<sup>8</sup>S. von Molnar, A. Briggs, J. Flouquet, and G. Remenyi, *Phys. Rev. Lett.* **51**, 706 (1983).

<sup>9</sup>T. Wojtowicz and A. Mycielski, *Physica* **117&118B**, 476 (1983).

<sup>10</sup>J. Jaroszynski and T. Dietl, *Solid State Commun.* **55**, 491 (1985).

<sup>11</sup>J. K. Furdyna, *J. Appl. Phys.* **53**, 7637 (1982).

<sup>12</sup>Y. Shapira, D. H. Ridgley, K. Dwight, A. Wold, K. P. Martin, J. S. Brooks, and P. A. Lee, *Solid State Commun.* **54**, 593 (1985).

<sup>13</sup>Y. Shapira, D. H. Ridgley, K. Dwight, A. Wold, K. P. Martin, and J. S. Brooks, *J. Appl. Phys.* **57**, 3210 (1985). Samples 3 and 7 in this reference correspond to samples No. 5-1 and No. 1-2 of the present paper, respectively.

<sup>14</sup>T. Dietl, J. Antoszewski, and L. Swierkowski, *Physica* **117&118B**, 491 (1983). See also, V. J. Goldman and H. D. Drew in *Proceedings of the 17th International Conference on the Physics of Semiconductors, San Francisco 1984*, edited by J. D. Chadi and W. A. Harrison (Springer, New York, 1985).

- p. 1427.
- <sup>15</sup>M. Sawicki, T. Dietl, J. Kossut, J. Igalson, T. Wojtowicz and W. Plesiewicz, *Phys. Rev. Lett.* **56**, 508 (1986); M. Sawicki, T. Dietl, and J. Kossut, *Acta Phys. Pol. A* **67**, 399 (1985).
- <sup>16</sup>J. Stankiewicz, S. von Molnar, and W. Giriat, *Phys. Rev. B* **33**, 3573 (1986).
- <sup>17</sup>D. M. Finlayson, J. Irvine, and L. S. Peterkin, *Philos. Mag. B* **39**, 253 (1979).
- <sup>18</sup>D. H. Ridgley, R. Kershaw, K. Dwight, and A. Wold, *Mater. Res. Bull.* **20**, 815 (1985).
- <sup>19</sup>Northern Analytical Laboratory, Amherst, NH 03031.
- <sup>20</sup>M. A. Novak, O. G. Symko, D. J. Zheng, and S. Oseroff, *J. Appl. Phys.* **57**, 3418 (1985).
- <sup>21</sup>D. Heiman, Y. Shapira, S. Foner, B. Khazai, R. Kershaw, K. Dwight, and A. Wold, *Phys. Rev. B* **29**, 5634 (1984).
- <sup>22</sup>J. A. Gaj, R. Planel, and G. Fishman, *Solid State Commun.* **29**, 435 (1979).
- <sup>23</sup>Y. Shapira, S. Foner, D. H. Ridgley, K. Dwight, and A. Wold, *Phys. Rev. B* **30**, 4021 (1984); Y. Shapira, S. Foner, P. Becla, D. N. Domingues, M. J. Naughton, and J. S. Brooks, *Phys. Rev. B* **33**, 356 (1986).
- <sup>24</sup>J. Stankiewicz and L. David, *J. Appl. Phys.* **56**, 3457 (1984).
- <sup>25</sup>D. L. Peterson, D. U. Bartholomew, U. Debska, A. K. Ramdas, and S. Rodrigues, *Phys. Rev. B* **32**, 323 (1985).
- <sup>26</sup>Y. Shapira and R. L. Kautz, *Phys. Rev. B* **10**, 4781 (1974).
- <sup>27</sup>See articles by N. F. Mott and H. Fritzsche, in *The Metal Non-Metal Transition in Disordered Systems*, Ref. 1 (particularly pp. 200–201 and 231).
- <sup>28</sup>A simplified expression for heavily doped semiconductors (B. I. Shklovskii and A. L. Efros, *Electronic Properties of Doped Semiconductors*, Ref. 2, p. 261) suggests that the shape of the band tail depends on the screening radius.
- <sup>29</sup>C. Haas, *Phys. Rev.* **168**, 531 (1968); *IBM J. Res. Dev.* **14**, 282 (1970); *CRC Crit. Rev. Solid State Sci.* **1**, 47 (1970).
- <sup>30</sup>Y. Ono and J. Kossut, *J. Phys. Soc. Jpn.* **53**, 1128 (1984).
- <sup>31</sup>Z.-Z. Gan and P. A. Lee (unpublished).
- <sup>32</sup>A. P. Grigin and E. L. Nagaev, *Pis'ma Zh. Eksp. Teor. Fiz.* **16**, 438 (1972) [*Sov. Phys.—JETP Lett.* **16**, 312 (1972)]. See also Nagaev's book (Ref. 6) p. 164 ff.
- <sup>33</sup>D. Heiman, P. A. Wolff, and J. Warnock, *Phys. Rev. B* **27**, 4848 (1983); T. Dietl and J. Spalek, *ibid.*, **28**, 1548 (1983).
- <sup>34</sup>R. L. Kautz and Y. Shapira, *Magnetism and Magnetic Materials*, Proceedings of the 20th Annual Conference on Magnetism and Magnetic Materials, AIP Conf. Proc. No. 24, edited by C. D. Graham, G. H. Lander, and J. J. Rhyne (AIP, New York, 1975), p. 42.
- <sup>35</sup>N. F. Mott, *Philos. Mag.* **6**, 287 (1961).
- <sup>36</sup>J. Kübler and D. T. Vigen, *Phys. Rev. B* **11**, 4440 (1975).
- <sup>37</sup>H. Fukuyama and K. Yosida, *J. Phys. Soc. Jpn.* **46**, 102 (1979).
- <sup>38</sup>D. J. Kim and B. B. Schwartz, *Phys. Rev. B* **15**, 377 (1977).
- <sup>39</sup>V. E. Zil'berverg and E. L. Nagaev, *Fiz. Tverd. Tela* **18**, 2499 (1976) [*Soviet Phys.—Solid State* **18**, 1460 (1976)].